MODELING CATALYZED GROWTH OF SINGLE-WALLED CARBON NANOTUBES

An Undergraduate Research Scholars Thesis

by

JENNI M. BEETGE

Submitted to Honors and Undergraduate Research
Texas A&M University
in partial fulfillment of the requirements for the designation as

UNDERGRADUATE RESEARCH SCHOLAR

Approved by
Research Advisor: Dr. Perla B. Balbuena

May 2013

Major: Chemical Engineering

TABLE OF CONTENTS

ABSTRACT

Modeling Catalyzed Growth of Single-Walled Carbon Nanotubes. (May 2013)

Jenni M. Beetge
Artie McFerrin Department of
Chemical Engineering
Texas A&M University

Research Advisor: Dr. Perla B. Balbuena
Artie McFerrin Department of
Chemical Engineering

Single walled carbon nanotubes (SWCNT's) are in high demand due to their wide range of applications. However, many applications are reserved for pure chirality SWCNT's because of the difference in properties associated with the twisting of the structure. Currently there are conflicting theories regarding the synthesis mechanism of SWCNT's. Understanding the effects of key parameters of SWCNT growth during chemical vapor deposition may enable manipulation of the process to produce SWCNT's with the desired chirality. This research project presents the results of classical molecular dynamics modeling of SWCNT nucleation and growth, focusing on the effects of nanoparticle-support interaction and precursor type on the chirality of the nanotube. Using SIMCAT, a reactive force field code, simulations are run for pure Ni nanoparticles with two types of carbon containing C2 precursor gas, each having five different support interaction energies, for three nanoparticle sizes. The same parameters were studied for different compositions of Ni and Co in bimetallic nanoparticles. The simulation results are used to visually examine the nucleation and growth processes as well as quantitatively determine statistics regarding carbon species inside and on the nanoparticle surface. The visualization results reflected the effects of kinetic and thermodynamic driving forces that cause

surface diffusion to dominate after carbon atoms filled the nanoparticle core through bulk diffusion. From the results we were also able to determine the probability curves and charts of carbon chain formation inside the nanoparticle and the hexamer and pentamer count on the nanoparticle surface. Analysis of these results suggests that carbide formation is not necessarily a prerequisite for carbon nanotube growth, which is one mechanism under debate. Furthermore, the nanoparticles displayed liquid-like solid behavior. While nanotube quality was hindered by the formation of bamboo growth due to strong metal-support interaction, higher quality nanotubes were observed for cases involving C2 precursor gas.

ACKNOWLEDGEMENTS

I would like to thank Dr. Balbuena and Dr. Diego Gomez-Gualdron at Texas A&M University for this exceptional opportunity. I would also like to thank Dr. Balbuena's research group, especially Juan Carlos Burgos, Rafael Callejas-Tovar, and José Leonardo Gómez Ballesteros for answering my frequent questions.

CHAPTER I

INTRODUCTION

The valuable semiconducting or metallic properties of Single Walled Carbon Nanotubes (SWCNT's) are in high demand for biomedical, electrical, and aerospace applications. The wide range of applications is due to variations in carbon nanotube structures, which dictate their electrical properties. For example, semiconducting carbon nanotubes have promising potential in biomedical nano-sensing applications [1]. The degree of structure twisting determines the properties of these conceptually cylindrical sheets of graphene, with a 30^{o} chiral angle separation between zig-zag, mostly semiconducting nanotubes and arm-chair, metallic nanotubes [2].

Currently the availability of this sought-after material is limited to industrial batch synthesis processes, which are not able to produce pure chirality carbon nanotubes and must be followed by nanotube separation methods. A significant barrier to achieving the required selectivity during nanotube production is inadequate understanding of the nanotube growth mechanism, specifically the effects of key growth parameters. Carbon nanotubes are commonly grown on a metallic nano-catalyst through chemical vapor deposition of a carbon-containing species, called the precursor gas. The nano-catalyst typically rests on a silicon-based support. Besides temperature and pressure, parameters that allow manipulation of the nanoparticle state, and therefore nanotube structure, include nanoparticle-support interaction, nano-catalyst composition, and precursor gas type.

Due to the nano-second timeframe of SWCNT production, and the nano-scale nature of the process, information obtained from experimental results is expensive and limited. Therefore, the objective of computational simulation methods is to direct or narrow experimentation of SWCNTs to facilitate the understanding of parameter effects on nanotube structure. Accordingly, the effects of nano-catalyst support have been investigated previously through molecular dynamics simulations. Diego Gómez-Gualdrón and Juan C. Burgos, of the research group of Dr. Perla B. Balbuena, studied the effects of nanoparticle-support interaction on nanotube growth. They determined that nanotube growth is generally promoted by the presence of a nano-catalyst support. However, they noted that a stronger nanoparticle/support interaction may hinder nanotube growth through wetting of the nano-catalyst on the support. Relatively high interaction strength was also observed to reduce the mobility of the nano-catalyst and disable the annealing effect that is necessary to produce high quality nanotubes [2, 3].

For unsupported catalysts, their previous results suggest an inverse template effect of the nanotube rim on the nanoparticle structure [2]. The direct template effect, in which the nanoparticle prescribes the nanotube rim structure, dominates during supported nanotube growth. This direct template effect may allow a desired structure to be imposed upon the nanotube. It was found that nano-catalyst-support interaction strength determines the degree of the direct template effect. These results suggest manipulation of the nanotube rim structure, and hence the nascent nanotube chirality, through the nanoparticle structure and support interaction. Therefore, it is import to understand the effects of manipulating nano-catalyst composition and support interaction to achieve desired nanotube chirality.

In this research project we aim to elucidate three important effects: one is associated with the effect of nano-catalyst-support interaction, the second with nature of the precursor gas, and the third is the composition of the metallic catalyst. This will be done by focusing on the characterization of the pathways followed by carbon atoms during single-walled carbon nanotube growth. We expect to answer questions related to the role of bulk versus surface diffusion for carbon atoms involved in the nucleation and growth of the nanotube, as well as the possibility of nano-catalyst carbide formation, by combination of carbon and metal atoms.

These details are important because they affect the mobility of the catalytic nanoparticle and therefore its effect on the structure of the growing nanotube. These effects are investigated for variable nano-catalyst/support interaction, precursor gas type, nano-catalyst size, and compositions of the nano-catalyst. Results are obtained using classical molecular dynamics modeling of SWCNT nucleation and growth. The reactive force field code used, SIMCAT, was developed by Dr. Balbuena's research group. This methodology is discussed further in the following section.

CHAPTER II

METHODS

Computational methods were utilized to obtain the results presented in this research project. Specifically, the growth of single walled carbon nanotubes on supported catalysts was simulated using the classical molecular dynamics code, SIMCAT, developed by Dr. Balbuena's research group [4]. This code applies input values of the parameter α in Equation 1 (discussed later) to model metal-support interaction [5]. Other energies that were not varied, such as metal-metal and carbon-carbon interactions are modeled within SIMCAT using the Sutton Chen potential and modified Brenner potential, respectively. The initial gas molecule velocity was set using Maxwell's speed distribution, and maintained at a temperature of 1000 K via Langevin dynamics. Pressure was kept at 11atm for C1, a precursor gas that produced one carbon atom upon catalysis of one gas molecule. For C2, a dimer producing gas, identical simulations were run for pressures of 11 atm as well as 5.5 atm. For each case, the precursor gas was introduced into the simulation box and monitored for 5 ns after the nanoparticle was equilibrated to establish the most stable structure.

To observe the effects of precursor gas type, nanoparticle size and metal-support interaction strength independently, 45 simulations were run. Each precursor gas type corresponded to fifteen cases of differing nanoparticle size (Ni32, Ni80 and Ni160) and interaction strength (Eadh = -0.16 eV, -0.26 eV, -0.43 eV, -0.70 eV and -1.39 eV). As a separate set of simulations that only contained C2 precursor gas, the effects of nanoparticle composition on carbon nanotube growth were studied by of varying nickel to cobalt ratios of a bimetallic nanoparticle of 32 atoms. Each

case of differing composition was run with two pairings of catalyst-support interaction values. Thus, the 18 bimetallic cases studied included pure Ni, pure Co, and Ni:Co ratios of 3:1, 1:1 and 1:3. The metal-support strengths applied to each case corresponded to α values of 0.14, 0.20 and 0.24, where α is a parameter of the following equation:

$$E_{ij} = \alpha V_{repulsion}(r_{ij}) - \alpha^{1.1} V_{attraction}(r_{ij}) \quad (1)$$

This equation expresses the interaction energy between the metal catalyst and support. The values chosen in our simulations are representative of the energies that correspond to commonly used support types and metal catalysts.

Data collected from the pure Ni simulations included a count of different carbon species within the nanoparticle as well as a dominance probability of each species (carbon chains or rings) within and on the surface of the nanoparticle. This was done through an algorithm that used a maximum bond length of 1.7 Å to identify carbon atoms bonded in chains or rings. Carbon atoms that were surrounded by at least six metal atoms no more than 2.5 Å away were considered as dissolved. The data collected from these algorithms were processed using graphical analysis.

Visual analysis, on the other hand, enabled a more direct observation of the possible mechanisms through which each precursor gas was catalyzed and incorporated into the carbon nanotube. Using Visual Molecular Dynamics software, we were able to identify a specific carbon atom by its index, and color code the atoms catalyzed at different stages of nucleation and growth to draw conclusions regarding the stability of the Ni-C core as well as typical pathways followed by the newly catalyzed atoms along the rim structure.

A slightly different approach was used to gather data for the bimetallic cases, such as the generation of mean squared velocity, pair radial distribution function and nanoparticle density graphs. The latter graph type was constructed using Z-Density, a code created by Dr. Balbuena's research group to determine the density of a particular atom type at each height interval perpendicular to the support. Along with the information provided by these graphs, visual analysis was performed for all of the bimetallic cases. Specific consideration was made to observe the behavior of catalyzed carbon atoms on the nanoparticle surface, to determine whether there is a preference for carbon to form structures around Ni, Co or interface areas. Additionally, in accordance with recent discoveries of "Bamboo growth" in carbon nanotubes, observations were made regarding the mechanism through which these structures were formed in certain cases [6]. Horizontal growth was similarly monitored in order to determine the conditions that favor this undesired occurrence.

CHAPTER III

RESULTS

Metal-support interaction effect on carbon species for pure Ni_{32}

This section discusses histograms that indicate carbon species dominance inside and on the surface of a pure, 32-atom nickel nanoparticle. The effect of the metal-carbon support interaction on the concentration of each species, from monomers to pentamers, is investigated. As a representative comparison of nucleation and growth behavior, C2 precursor gas data are chosen. The effects of the two precursor gases C1 and C2 are then compared for overall species dominance at each metal/support interaction energy, E_{adh}. Nano-catalyst-support interaction energies of -0.16eV, -0.26eV, -0.43eV, -0.70eV and -13.9eV are chosen for this study, and correspond to α-values of 0.10, 0.14, 0.20, 028, 0.42, respectively.

Nucleation stage

Once a C2 precursor gas molecule is catalyzed, the surface deposited dimer has to split into two carbon atoms for bulk diffusion or remain on the nanoparticle surface. During early nucleation, the driving force for bulk diffusion overcomes the energy barrier and causes the dimer bond to break. As a result of the individual diffusion of carbon atoms into the nanoparticle, monomers are the most dominant species inside the nanoparticle (Fig. 1).

Within the nanoparticle, the probability of dominance decreases as carbon chain length increases. Larger carbon structures are less prevalent inside the nanoparticle due to diffusion barriers separating carbon atoms and possibly the breaking of larger chains due to nanoparticle atom

mobility. Accordingly, each interaction value in Figure 1 displays relatively low trimer, tetramer and pentamer counts inside the nanoparticle. At the highest metal-substrate interaction, the particle flattens and cannot contain the larger carbon structures.

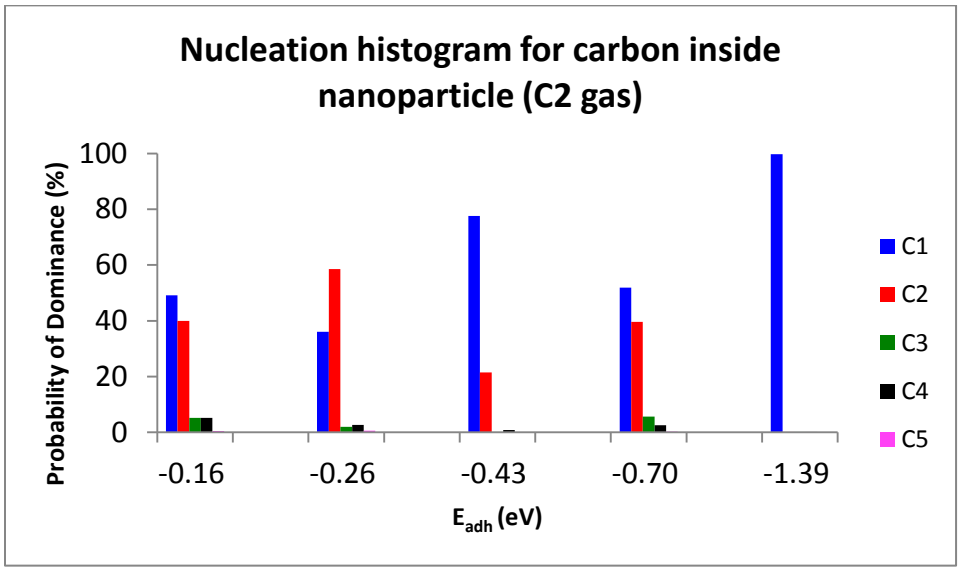

Figure 1. Histograms show the probability for a given carbon species of being the dominant species inside the nanoparticle during nanotube nucleation for different values of E_{adh}.

While monomer abundance was shown to dominate the nanoparticle interior for most metal-support cases, dimers were shown to be the most prevalent species on the nanoparticle surface (Fig. 2). As the nucleation stage progresses, the driving force for bulk diffusion is significantly lower, possibly due to saturation of the nanoparticle. Some of the dissolved carbon atoms resurface and catalyzed dimers may start to remain on the surface, which accounts for the abundance of dimers on the nanoparticle surface. Larger carbon chains are also observed more on the nanoparticle surface than inside the nanoparticle, possibly suggesting that the surface is more stable than the interior.

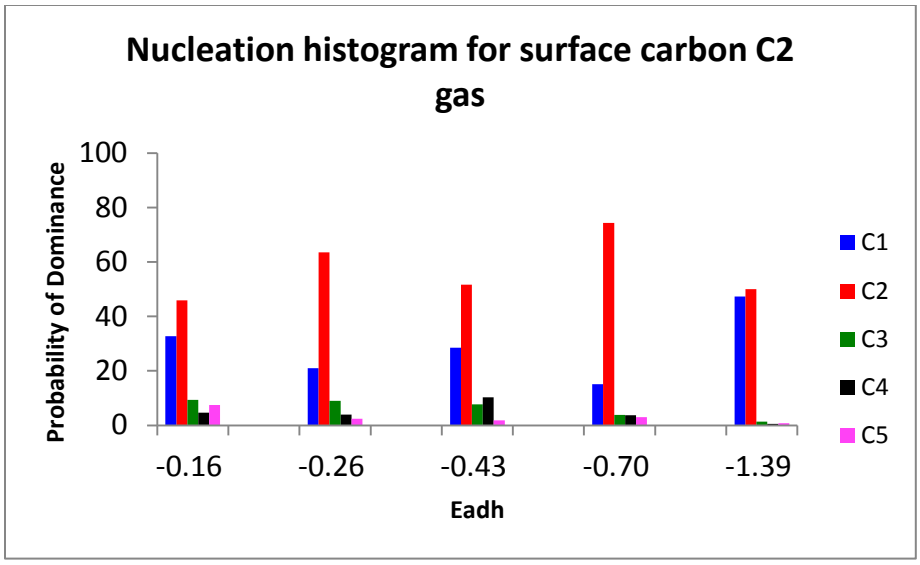

Figure 2. Histograms show the probability for a given carbon species of being the dominant species outside the nanoparticle during nanotube nucleation for different values of E_{adh}.

Growth stage

After the nanotube cap is formed, the structure lifts from the surface as additional carbon atoms attach to the cap rim. The nanoparticle undergoes rearrangement according to its interaction with the support. At the lowest metal/support interaction values, the nanoparticle volume to surface ratio was more conducive for carbon chains, especially dimers. As the support interaction increased, the wetting of the nanoparticle to the support also increased, limiting the volume available for carbon species to form and prevail. As shown in Figure 3, no carbon species are able to be contained within the nanoparticle at the highest interaction value of -1.39eV.

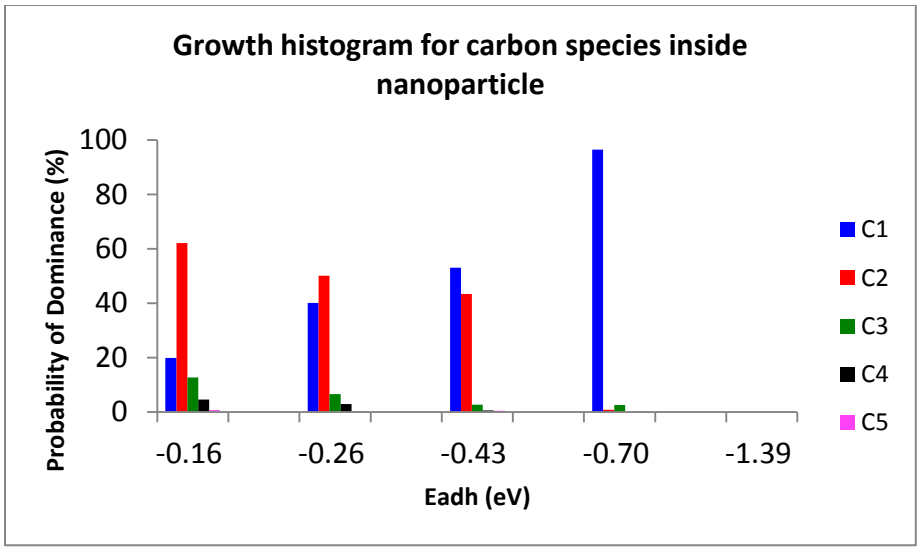

Figure 3. Histograms show the probability for a given carbon species of being the dominant species inside the nanoparticle during nanotube growth for different values of $E_{adh.}$

In contrast to the previous histograms, carbon species dominance on the nanoparticle surface does not follow a clear trend (Figure 4). At the strongest interaction value, -1.39eV, monomers are the most abundant species. Visualization of the simulations confirms that only the nanotube rim is in contact with the nanoparticle, suggesting that the rim area is unstable and causes dimers that attach to the rim to split. An interesting phenomenon is observed in which the next strongest interaction value, -0.70eV, allows for all five carbon species to be prevalent on the surface, similar to the behavior at the two weakest interaction energies. Visualization of this case reveals that a phenomenon called Bamboo growth (discussed in the Bimetallics section) occurred, in which a carbon network forms across the nanotube rim, on the nanoparticle surface. This accounts for the presence of larger carbon chains on the nanoparticle surface during growth, and is shown in later sections to be the result of stronger metal- support interactions.

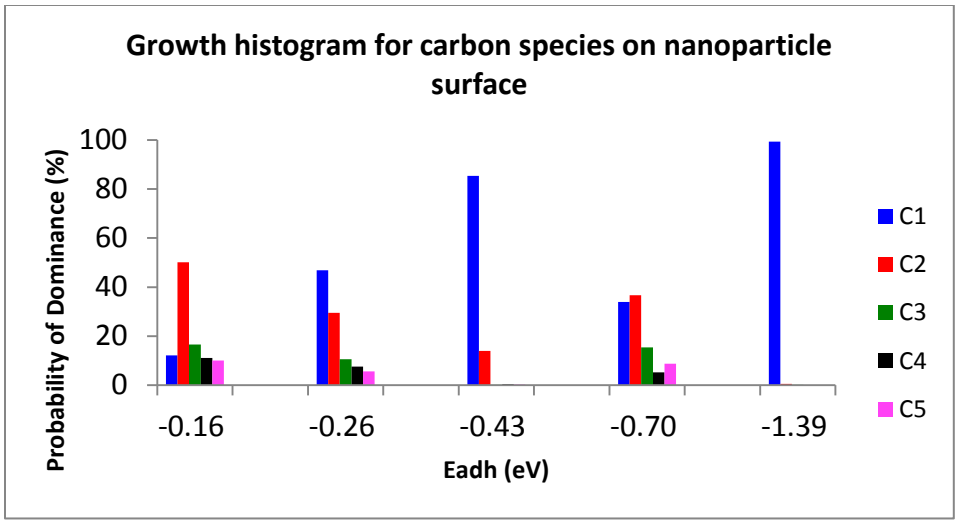

Figure 4. Histograms show the probability for a given carbon species of being the dominant species on the surface of the nanoparticle during nanotube growth for different values of $E_{adh.}$

Overall dominance probability

Carbon species dominance inside the nanoparticle throughout the entire process of nucleation and growth are displayed for C2 gas at 11atm in Figure 5, and for C1 gas at 11atm in Figure 6. From Figure 5, it is evident that the dominance of larger species, especially dimers, becomes less probable with increasing interaction strength. At -0.43eV, the monomer dominance starts to become the most prevalent. However, dimers maintain a significant presence (less than 35% dominance probability) inside the nanoparticle, even at the highest interaction strength.

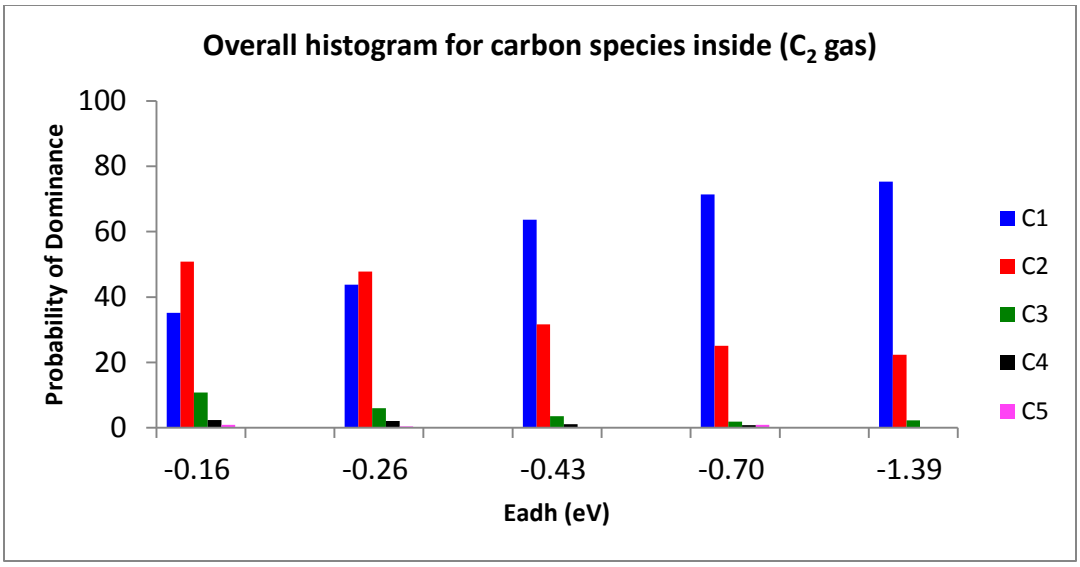

Figure 5. Precursor C_2 gas - Histograms show the probability for a given carbon species of being the dominant species inside the nanoparticle throughout nanotube nucleation and growth for different values of $E_{adh.}$

The overall trends for simulations of C1 precursor gas differed significantly from those of C2 gas, as seen by comparison of Figures 5 and 6. For the entire range of support interaction values, C_1 gas promoted the dominance of larger carbon structures inside the nanoparticle. At the lowest interaction strength, E_{adh}= -0.16eV, dimers and trimers have the highest probability of dominance, at 30%. The four higher interaction strengths all indicate dimers to be the dominant species. Monomer dominance fluctuates and has an overall increase from 14% to 26%, in the case of C1 gas. In contrast, the use of C2 gas caused a more steady increase in monomer dominance, from ~35% to 75%, over the range of increasing E_{adh} values. Whereas Figure 5 showed a clear trend of increasing monomer dominance with interaction energy for the C_2 precursor gas, Figure 6 suggests that C_1 gas has a stabilization effect on the nanoparticle, since dominance of each species is relatively constant throughout the range of E_{adh} values. This stabilization effect is likely to be the result of slower catalysis rate, and is discussed further in the Carbon Dissolution and Resurfacing Rates subsection.

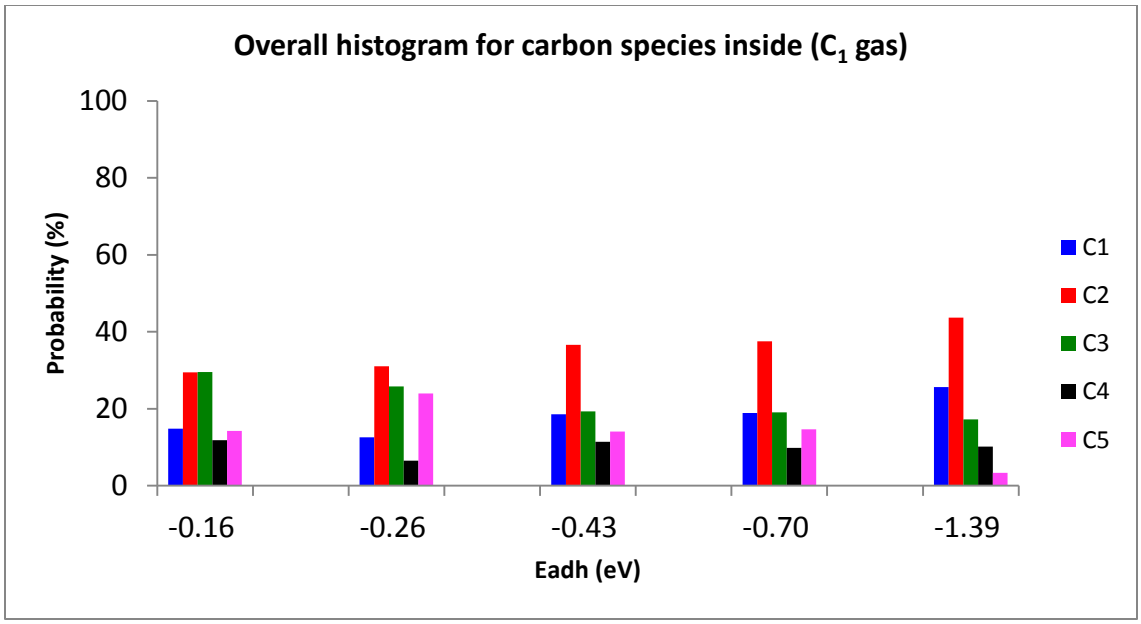

Figure 6. Precursor C_1 gas - Histograms show the probability for a given carbon species of being the dominant species inside the nanoparticle throughout nanotube nucleation and growth for different values of $E_{adh.}$

The histogram for carbon species on the nanoparticle surface with C_2 precursor gas is shown in Figure 7. Both monomer and dimer probabilities of dominance fluctuate, and dimers are shown to be the most abundant species at interaction strengths of -0.16eV, -0.26eV and -0.70eV. The resemblance between the resulting effects of the other two values, -0.43eV and -1.39eV, or the unique behavior at -0.70eV, is once again observed. Very low dominance probabilities of trimers, tetramers and pentamers occur on the nanotube surface during nanotube growth and nucleation at the highest interaction strength. This indicates that the growing nanotube has a lower degree of contact with the nanoparticle and a higher species incorporation rate, at -1.39eV.

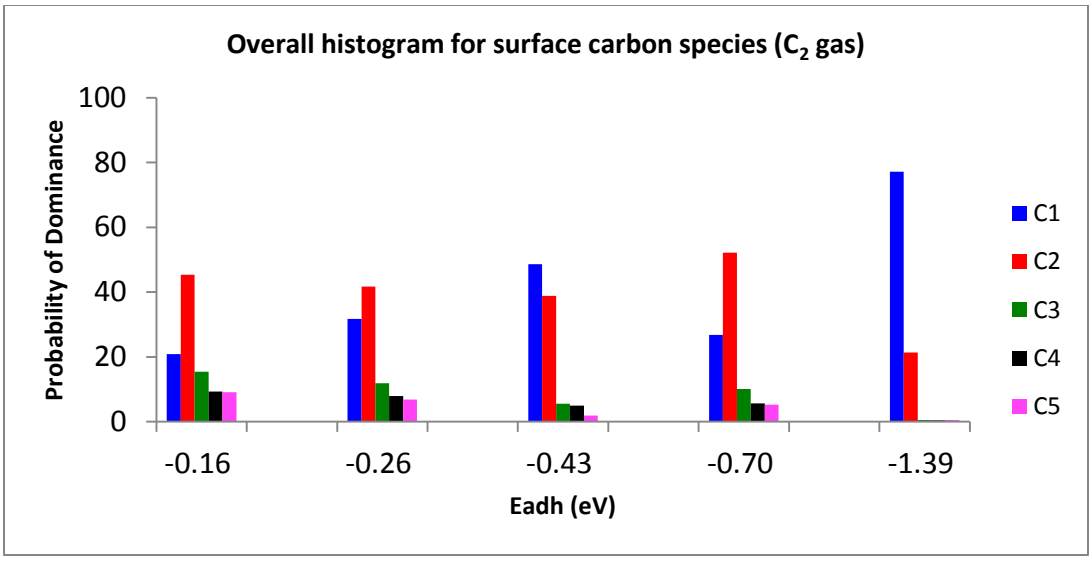

Figure 7. Precursor C_2 gas - Histograms show the probability for a given carbon species of being the dominant species on the surface of the nanoparticle throughout nanotube nucleation and growth for different values of E_{adh}

In the case of C1 precursor gas, Figure 8 shows that monomers are the dominant species on the nanoparticle surface for all interaction strengths. The larger carbon species have significant dominance, even at E_{adh}=-1.39eV (>5%). This suggests that the C1 gas causes slower incorporation of carbon structures into the nascent nanotube cap. A faster incorporation rate is expected in the case of C2 gas because dimers are added to the structure upon contact with the nanoparticle.

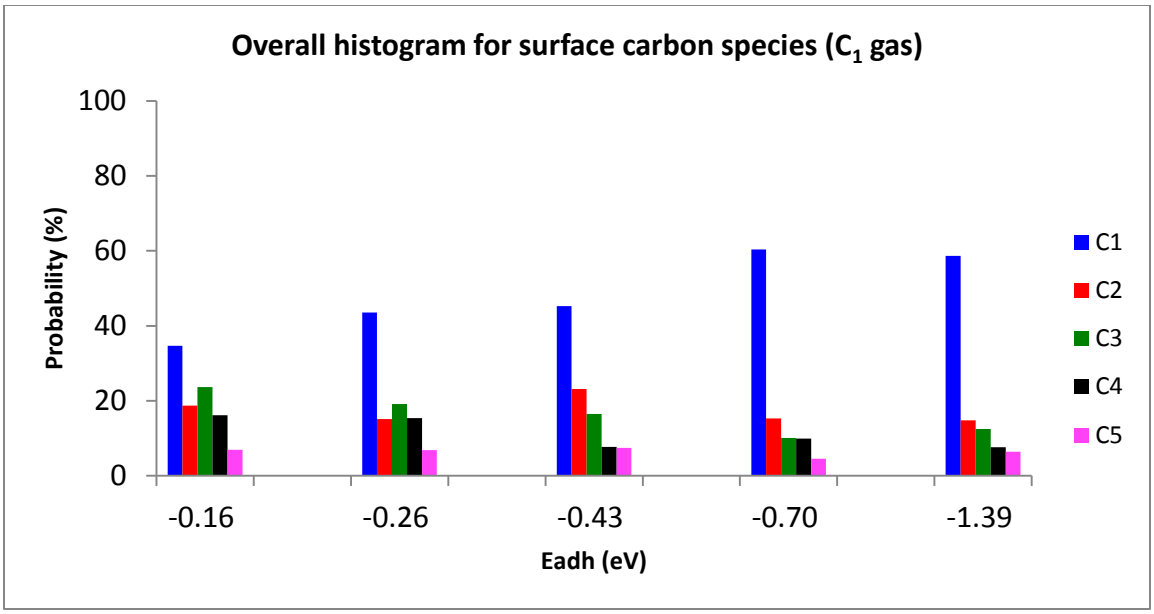

Figure 8. Precursor C_1 gas - Histograms show the probability for a given carbon species of being the dominant species on the surface of the nanoparticle throughout nanotube nucleation and growth for different values of E_{adh}

Carbon dissolution and resurfacing rates for pure Ni

Carbon diffusion rates were determined by counting the number of carbon atoms inside and on the nanoparticle surface at every half pico-second of simulation. Graphical analysis of the data enabled estimations of nanoparticle saturation point (ts), the onset of nanotube cap separation and growth (tt), the number of carbon atoms dissolved at the corresponding moment in time (nd) and catalyzed (nc). The average number of dissolved carbons is recorded for two time frames, the first being from the saturation point to the onset of growth, and the second was evaluated from the latter (tt) until the end of the simulation (5,000 ps). Catalysis rate, Rc, as well as catalysis frequency, τc, was determined for the two time frames as well. The results of this analysis are presented in Tables 1 and 2 for comparison of C1 gas at 11atm and C2 gas at 5.5 atm.

Table 1: Pure Ni with C1 at 11atm

Ni32											
α	ts (ps)	tt (ps)	nd(ts)	nout(ts)	nc (tt)	nd(I)av	nd(II)av	Rc(I)	Rc(II)	τc(I) (ps)	τc(II) (ps)
0.10	182.00	864.00	14	30	106	11	10	0.113	0.008	8.86	128.21
0.14	194.50	263.00	13	25	54	11	10	0.169	0.047	5.92	21.51
0.20	32.50	16.00	3	11	40	4	8	0.188	0.042	5.32	23.58
0.28	165.00	178.50	6	30	38	6	6	0.182	0.053	5.49	18.94
0.42	79.50	385.00	4	22	64	4	1	0.152	0.064	6.56	15.75

Ni80											
α	ts (ps)	tt (ps)	nd(ts)	nout(ts)	nc (tt)	nd(I)av	nd(II)av	Rc(I)	Rc(II)	τc(I) (ps)	τc(II) (ps)
0.10	264.50	500.50	35	69	176	59	37	0.280	0.017	3.57	58.48
0.14	173.00	444.00	36	38	350	38	38	0.258	0.026	3.87	38.31
0.20	254.00	488.50	39	51	134	39	38	0.211	0.048	4.75	20.83
0.28	194.50	464.00	29	25	120	32	32	0.200	0.079	5.00	12.67
0.42	261.00	500.50	34	50	130	33	22	0.207	0.095	4.84	10.48

Ni160											
α	ts (ps)	tt (ps)	nd(ts)	nout(ts)	nc (tt)	nd(I)av	nd(II)av	Rc(I)	Rc(II)	τc(I) (ps)	τc(II) (ps)
0.10	639.50	1526.00	100	156	380	98	95	0.193	0.017	5.18	58.82
0.14	675.00	1515.00	103	167	350	96	93	0.177	0.019	5.64	53.76
0.20	458.50	856.00	98	128	302	94	92	0.263	0.039	3.80	25.91
0.28	369.00	566.50	90	120	260	90	87	0.330	0.082	3.03	12.22
0.42	276.50	664.50	89	55	262	89	67	0.292	0.118	3.42	8.47

Table 2: Pure Ni with C2 at 5.5atm

Ni32 Half Density											
α	ts (ps)	tt (ps)	nd(ts)	nout(ts)	nc (tt)	nd(I)av	nd(II)av	Rc(I)	Rc(II)	τc(I) (ps)	τc(II) (ps)
0.10	212.50	2191.00	12	26	138	11	10	0.052	0.002	19.08	588.24
0.14	270.50	1519.50	12	18	70	10	8	0.033	0.025	30.58	39.68
0.20	245.00	1001.00	9	19	70	8	9	0.058	0.026	17.39	38.91
0.28	114.00	-	7	5	-	-	-	-	-	-	-
0.42	192.50	1154.00	7	17	82	4	1	0.068	0.035	14.71	28.65

Ni80 Half Density											
α	ts (ps)	tt (ps)	nd(ts)	nout(ts)	nc (tt)	nd(I)av	nd(II)av	Rc(I)	Rc(II)	τc(I) (ps)	τc(II) (ps)
0.10	415.50	1536.00	41	45	200	39	2	0.111	0.017	9.03	57.80
0.14	235.50	2110.50	35	25	188	39	37	0.072	0.014	13.83	69.44
0.20	424.50	1500.50	36	36	174	37	34	0.107	0.023	9.33	43.67
0.28	336.00	1235.00	29	21	148	34	31	0.100	0.041	9.99	24.63
0.42	403.50	693.50	32	34	102	31	18	0.108	0.067	9.23	14.86

Ni160 Half Density											
α	ts (ps)	tt (ps)	nd(ts)	nout(ts)	nc (tt)	nd(I)av	nd(II)av	Rc(I)	Rc(II)	τc(I) (ps)	τc(II) (ps)
0.10	422.00	804.50	93	47	260	96	99	0.206	0.075	4.85	13.26
0.14	683.50	900.50	104	74	228	102	99	0.139	0.088	7.17	11.40
0.20	441.00	1097.00	97	43	264	96	91	0.170	0.044	5.88	22.88
0.28	625.50	916.00	96	66	222	97	90	0.147	0.066	6.81	15.24
0.42	501.50	1000.50	97	43	234	90	76	0.160	0.094	6.26	10.68

The use of C1 precursor gas resulted in less residence time between saturation and the onset of nanotube growth (separation of cap from nanoparticle) with increasing metal/support interaction energy. This observation suggests that an increase in nanoparticle-support interaction facilitates faster incorporation of surface atoms into the nanotube cap network. Thus, as the α-value increases, the nanoparticle-support wetting increases, flattening the nanoparticle and allowing closer encounters between surface carbon atoms. However, this trend is not as clearly observed for cases involving C2 precursor gas with larger nanoparticle sizes (Ni80 and Ni160). Instead,

the saturation and nucleation termination points fluctuate as support interaction energy is increased. The corresponding residence times similarly fluctuate without a clear trend.

Another observation that results from the comparison of these data is the decrease in catalysis rate between the first timeframe, essentially cap nucleation, and the second timeframe, the onset of growth. Therefore, within this residence time the catalysis of carbon atoms decreases for all cases and precursor gas types except Ni32 with C2 gas. This sudden decrease with respect to time is likely the result of the transition from accumulation of surface carbons to cap lift off, at which point less nanoparticle surface is exposed to the gas and a significantly lower amount of carbon atoms are deposited on the surface, before being incorporated into the rim.

Nanotube quality for pure Ni

Bamboo growth, mentioned earlier, obstructs carbon nanotube quality. Twelve cases of bamboo growth were observed among the Ni simulations, ranging over all precursor gases and pressures. Snapshots of these simulations are displayed in Figure 9. Bamboo growth was only observed at middle to highest metal-support interaction values (α=0.20, 0.28. 0.42). A few full density (Pressure of 11atm), C2 gas cases and corresponding C1 cases resulted in identical growth. For example, Figure 9 G represents the resulting growth of C1 as well as C2 (11 atm) gas, with Ni80 nanoparticle and interaction value of 0.28. Furthermore, Figure 9, J displays bamboo growth for the same nanoparticle size and support interaction, using C2 at 5.5 atm. A similar trend was identified for the case of Ni80 at α=0.42 (Figure 9, H and I). Among the 45 pure Ni simulations, 14 total bamboo growth cases were observed. Although the nanotube structures for these case sets are not identical, the results show that bamboo growth was not affected by precursor gas

type. Therefore, the bamboo growth mechanism is expected to be independent of differences in rim attachment (single carbon atom or dimer). Further discussion regarding bamboo growth mechanism follows with the Bimetallics discussion.

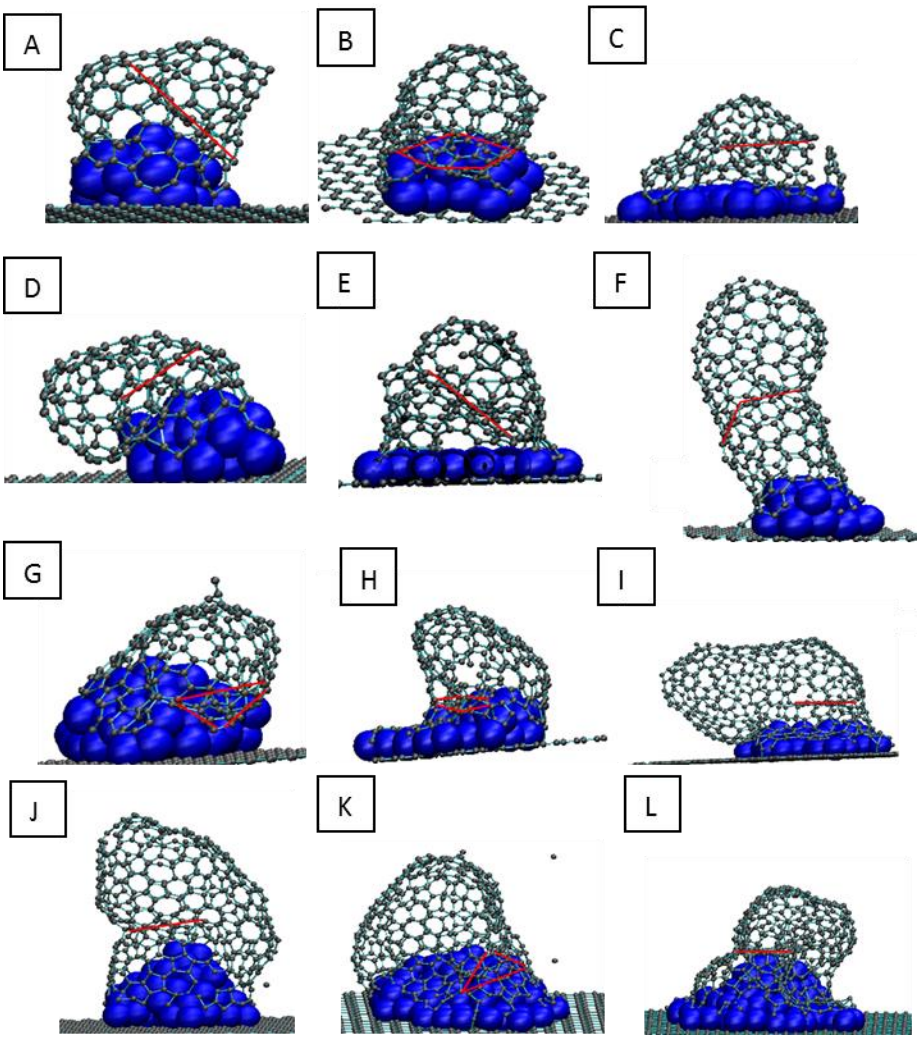

Figure 9. Snapshots of bamboo cases for pure Ni nanoparticle; A) Ni32 using C1 precursor gas at a nanoparticle-support interaction coefficient of 0.20; B) Ni32 using C1 at 0.28; C) Ni32 using C1 precursor gas at 0.42; D) Ni32 using C2, 5.5 atm, at interaction coefficient of 0.28; E) Ni32 using C2, 5.5 atm, at 0.42; F) Ni32 using C2, 11atm, at 0.28; G) Ni80 using C1 (identical for C2 at 11atm) at 0.28; H) Ni80 using C1 (identical for C2 at 11atm) at 0.42; I) Ni80 using C2, 5.5atm, at 0.42; J) Ni80 using C2, 5.5atm, at 0.28; K) Ni160 using C1 at 0.42; L) Ni160 using C2, 5.5atm, at 0.42.

In addition to the absence of bamboo growth, high quality nanotubes are characterized by the quantity of hexagons present in their structure. Comparison of this aspect of nanotube quality is presented in Figure 10, for each nanoparticle size, precursor gas type and metal-support interaction value, α, of 0.10, 0.20 and 0.42. These values are chosen to represent relatively weak, medium and strong interactions with the support, respectively.

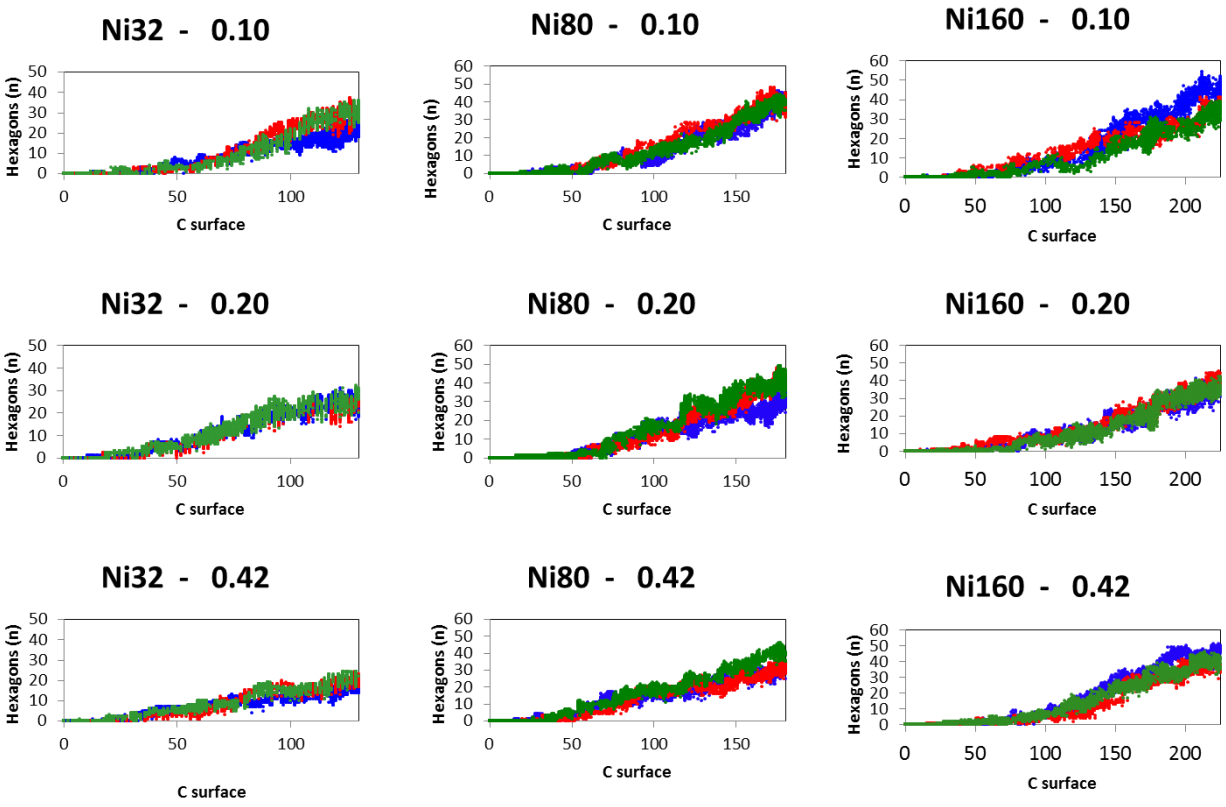

Figure 10. Number of hexagons as a function of the number of carbon atoms on the nanoparticle surface. C1 precursor gas at 11atm is displayed in blue, C2 at 11atm is displayed in red, and C2 at 5.5 atm is displayed in green.

A slight preference for hexagons is observed with the use of C2 gas at 5.5atm, in the cases of Ni32 and Ni80 (with equally strong preference with C1 gas at the interaction value of 0.10). The largest nanoparticle size, Ni160, is shown to have better nanotube quality at C1 precursor gas.

The success of the C2 precursor gas at 5.5 atm can be attributed to the mechanism by which dimers are attached to the rim structure, possibly favoring hexagon formation over other polygons. (This mechanism was investigated, and results are presented in the Dimer Mechanism section.) At the larger nanoparticle size, however, C1 gas produces carbon nanotubes with a slightly higher hexagon count. The high surface area facilitates catalysis, as shown in Tables 1 and 2, through an overall increase in catalysis rate as nanoparticle size increases. Since the C2 gas delivers two carbon atoms for each catalyzed molecule, even at half of the C1 gas pressure, the rate increase due to the combination of size and abundance of carbon inhibits defect annealing. Thus, the network of polygons is formed faster with C2 gas and does not have adequate time to rearrange into a more stable structure of mostly hexagons. It should be noted that pentagon stability has been found to be similar in magnitude, depending on the arrangement of the metal atoms in the underlying nanoparticle [2].

Mechanisms of dimer rim incorporation

It is expected that dimer addition to the rim structure facilitates the formation of hexagons and pentagons. To understand this mechanism, several dimers were identified and colored to track their paths as the simulation progressed. Visualization snapshots are presented in Figure 11. This visualization technique was used to monitor the full density C2 simulation set. Two pathways were observed, depending on the attachment site. One mechanism begins when, upon catalysis, one of the dimer carbons bonds as a chain to another carbon atom at the rim. The second dimer carbon then migrates to the rim, maintaining the dimer bond, until it completes a polygon with adjacent carbon atoms at the rim. Again depending on the attachment site, this polygon may be a pentagon, hexagon or heptagon, among other less frequently observed

polygons. The other observed mechanism was the immediate incorporation of the dimer to complete a pentagon or hexagon at the rim. Thus, the proposed mechanism was observed, although nanoparticle instability may cause this mechanism to apply less frequently. It is worth mentioning that nanoparticle stability was significant enough, even at the weakest E_{adh} value (Fig. 11), to allow a few dimers to remain intact as they advance along the nanotube structure.

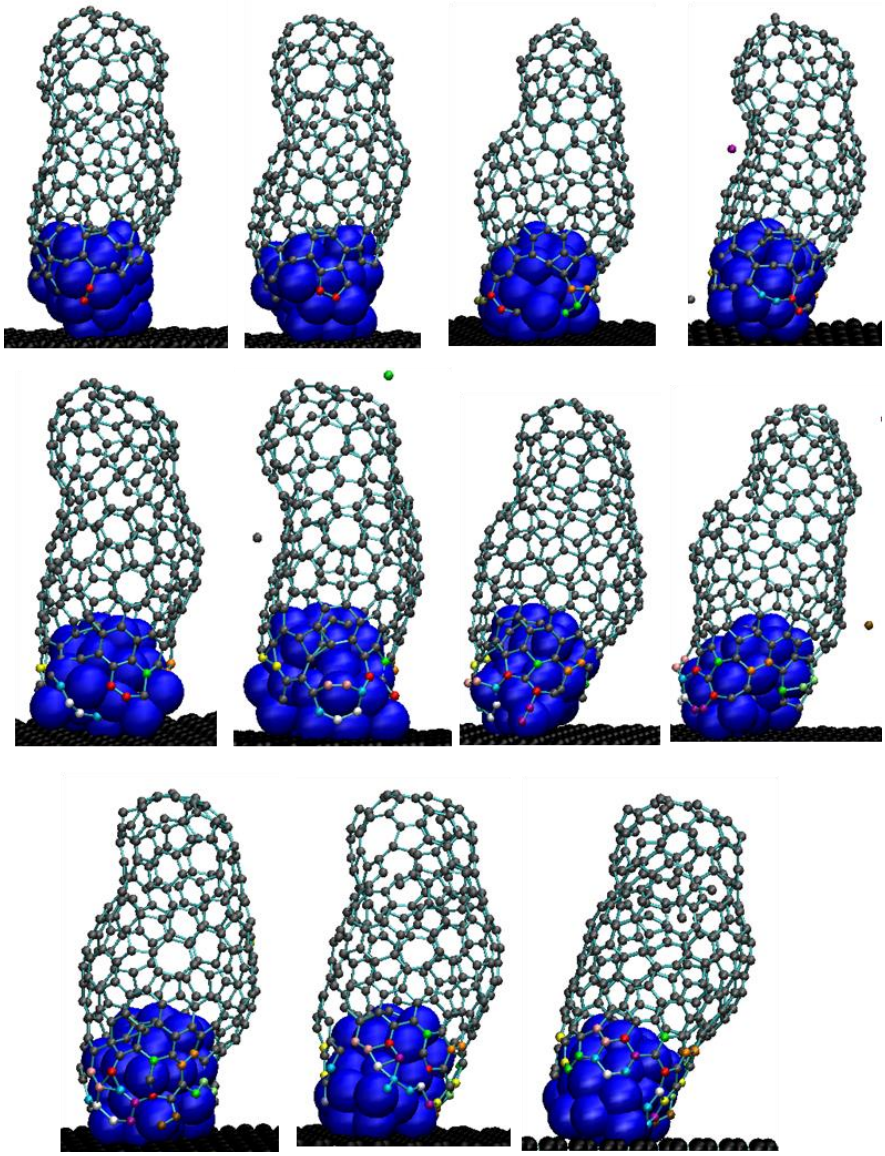

Figure 11. Series of simulation snapshots, progressing from left to right across each row of snapshots, of dimer to rim addition for Ni_{32} at -0.16 eV; Each dimer is identified with a color (red, orange, green, light blue (used for two dimers), white, pink, yellow, purple and brown).

Cobalt and nickel bimetallic nanoparticles

The resulting carbon nanotubes grown during sets of simulations, varying Co-Ni nanoparticle composition, were visually examined for quality and quantitatively analyzed to determine trends in nanoparticle mobility and component density gradients. All of the bimetallic simulations were

specified with C2 gas at 5.5atm, on a 32 atom nanoparticle. The goal for this analysis was to determine if nanoparticle state varies with composition, and whether horizontal growth and bamboo growth were more likely to occur when the nanoparticle is bimetallic. Visualization results for each case of Ni-Co composition, and the corresponding metal-support interaction value, are displayed in Figures 12 and 13, and summarized in Tables 3 and 4.

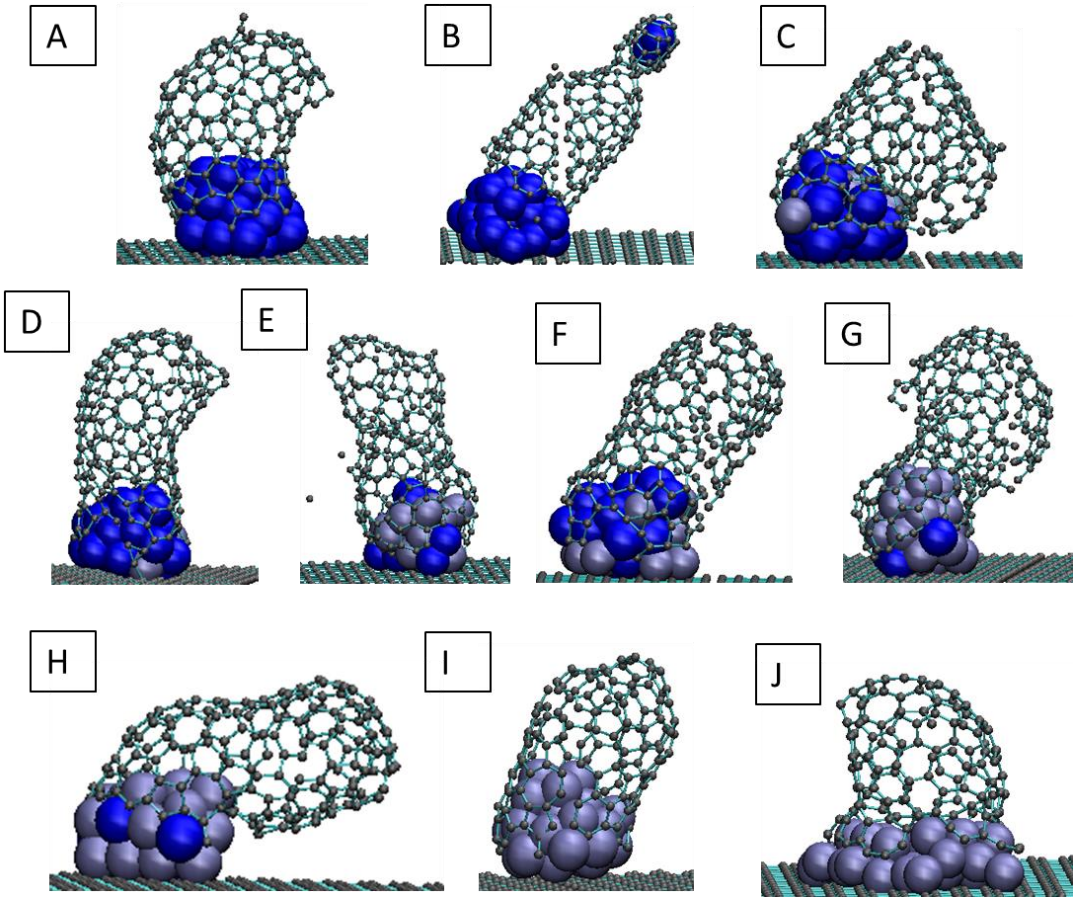

Figure 12. End of nanotube growth snapshots of bimetallic nanoparticle simulation set; Each case is labeled according to composition and metal-support interaction energy as presented in Table 3.

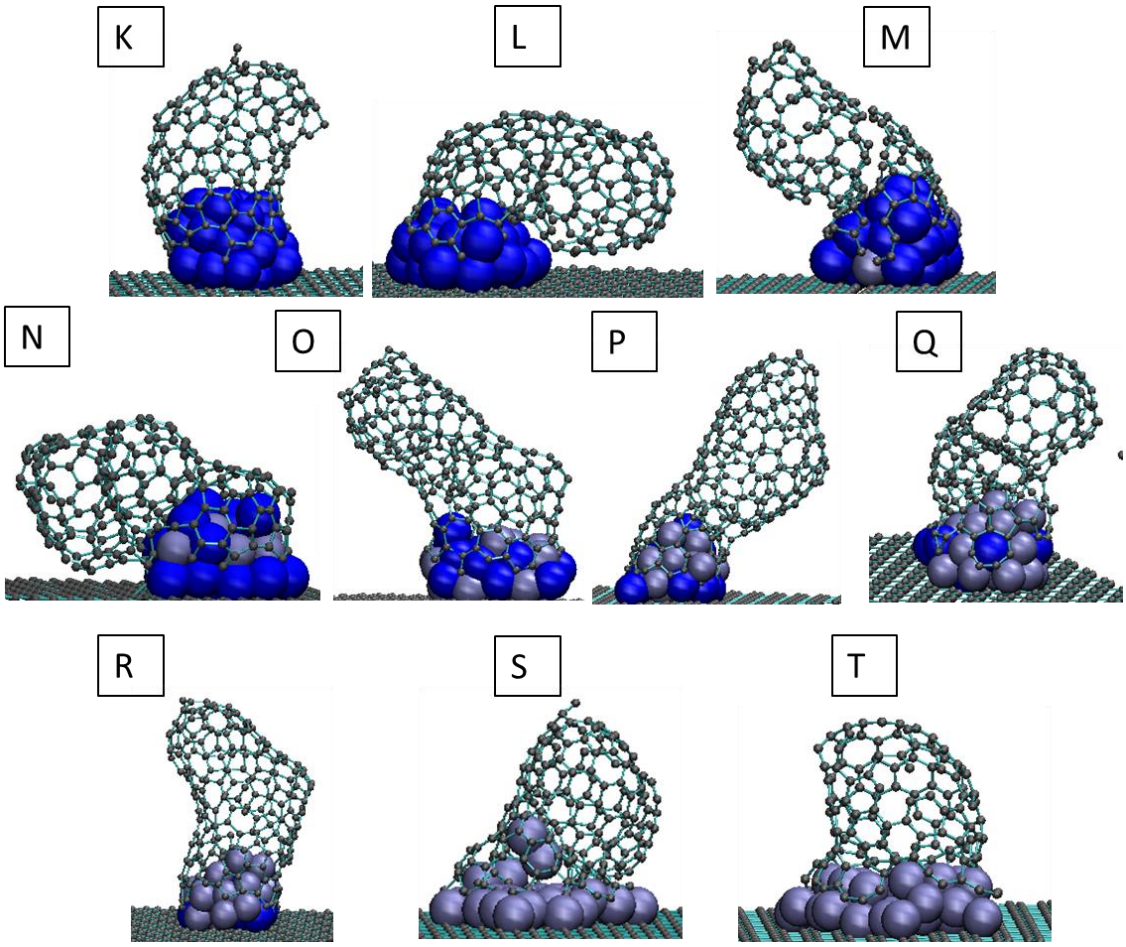

Figure 13. End of nanotube growth snapshots of bimetallic nanoparticle simulation set; Each case is labeled according to composition and metal-support interaction energy as presented in Table 4.

Within the 12 bimetallic cases, 7 nanotubes grew horizontally and 11 nanotubes were characterized by bamboo growth. Similarly, the pure Ni and pure Co cases presented in the table displayed bamboo growth in all four cases whereas horizontal growth was observed in three of the four cases. The strong tendency for bamboo growth to occur at medium to high metal-support interaction energies, observed in the pure Ni cases, is confirmed for bimetallic nanoparticles.

Table 3: Summary of results with alternating α-values 0.20 and 0.14

	Horizontal growth	Bamboo growth	Nucleation preference	First nucleating ring
A) Ni32 - 0.20	Y	Y	N/A	Pentagon
B) Ni32 - 0.14	No	Y	N/A	Pentagon
C) Co8 (0.14) - Ni24 (0.20)	Y	Y	Interface	Pentagon
D) Co8 (0.20) - Ni24 (0.14)	Y	Y	Interface	Pentagon
E) Co16 (0.14) - Ni16 (0.20)	No	Y	Interface	Pentagon
F) Co16 (0.20) - Ni16 (0.14)	Y	Y	No preference	Hexagon
G) Co24 (0.14) - Ni8 (0.20)	No	Y	Interface	Heptagon
H) Co24 (0.20) - Ni8 (0.14)	Y	Y	Interface	Pentagon
I) Co32 - 0.14	Y	No	N/A	Pentagon
J) Co32 - 0.20	Y	Y	N/A	Pentagon

Table 4: Summary of results with alternating α-values 0.20 and 0.24

	Horizontal growth	Bamboo growth	Nucleation preference	First nucleating ring
K) Ni32 - 0.20	Y	Y	N/A	Pentagon
L) Ni32 - 0.24	Y	Y	N/A	Pentagon
M) Co8 (0.24) - Ni24 (0.20)	Y	Y	Interface	Hexagon
N) Co8 (0.20) - Ni24 (0.24)	Y	Y	No preference	Pentagon
O) Co16 (0.24) - Ni16 (0.20)	Y	Y	No preference	Heptagon
P) Co16 (0.20) - Ni16 (0.24)	No	Y	Interface	Pentagon
Q) Co24 (0.24) - Ni8 (0.20)	No	Y	Interface	Heptagon
R) Co24 (0.20) - Ni8 (0.24)	No	No	Interface	Pentagon
S) Co32 - 0.24	Y	Y	N/A	Hexagon
T) Co32 - 0.20	Y	Y	N/A	Pentagon

Comparison of the data in Tables 3 and 4 suggests that horizontal growth was less likely to occur at higher metal-support interaction energies for bimetallic nanoparticles. In contrast, horizontal

growth seems to be less likely at low metal-support interaction energies in the pure Ni case. Visual comparison of the pure Ni_{32} simulation set confirms that horizontal growth was not observed at low interaction with the support.

Mean Squared Displacement, Z-density, and Pair Radial Distribution Function

Simulation data for the bimetallic nanoparticle sets were processed to allow investigation of nanoparticle state, through Mean Squared Displacement (MSD) graphs, and composition and density gradients, from Z-density and Radial Pair Distribution Function (RPDF) analyses. Nanoparticle growth and equilibration, wherein the nanoparticle was allowed to rearrange according to metal-support interaction energies without introduction to precursor gas, were evaluated separately.

The complete sets of MSD graphical analysis are presented in Figures 14 and 15, which indicate the diffusion of atoms within each of the nanoparticles. Equilibration data show that when Ni is at the lowest alpha value (0.14), and Co is at 0.20, Ni has a higher mobility than Co. In other words, when nickel-support interaction is lower than cobalt, Ni is the more mobile component. In contrast, when Co is at the highest alpha value (0.24) and Ni is at 0.20, Co has a higher mobility than Ni. That is, cobalt has a higher mobility when its support-interaction is higher than nickel. A higher mobility is expected when support-interaction is lowered. The interesting behavior of Co atoms can be explained by comparison of Ni and Co atomic properties: Since Co is heavier (Co atomic weight is 58.9g/mol while Ni atomic weight is 58.7 g/mol), the combination of higher atomic weight and stronger interaction energy necessitates rearrangement of Co atoms to the bottom of the nanoparticle.

Furthermore, it is observed in the cases of Co 0.14 – Ni 0.20 and Co 0.24 – Ni 0.20 that the mobility of the weaker-interaction component increases as the concentration of this same component is increased. This behavior is expected, as the ability of atoms to travel is enhanced when fewer atoms are present which have strong interaction with the support.

Comparison of equilibration and growth diffusion suggest that the introduction of precursor gas has some effect on nanoparticle mobility, although the mobilities are still on the same order of magnitude, ranging from 10^{-6} to 10^{-7} Å²/ps. The bimetallic nanoparticles are generally slightly less mobile during growth than the pure nanoparticles.

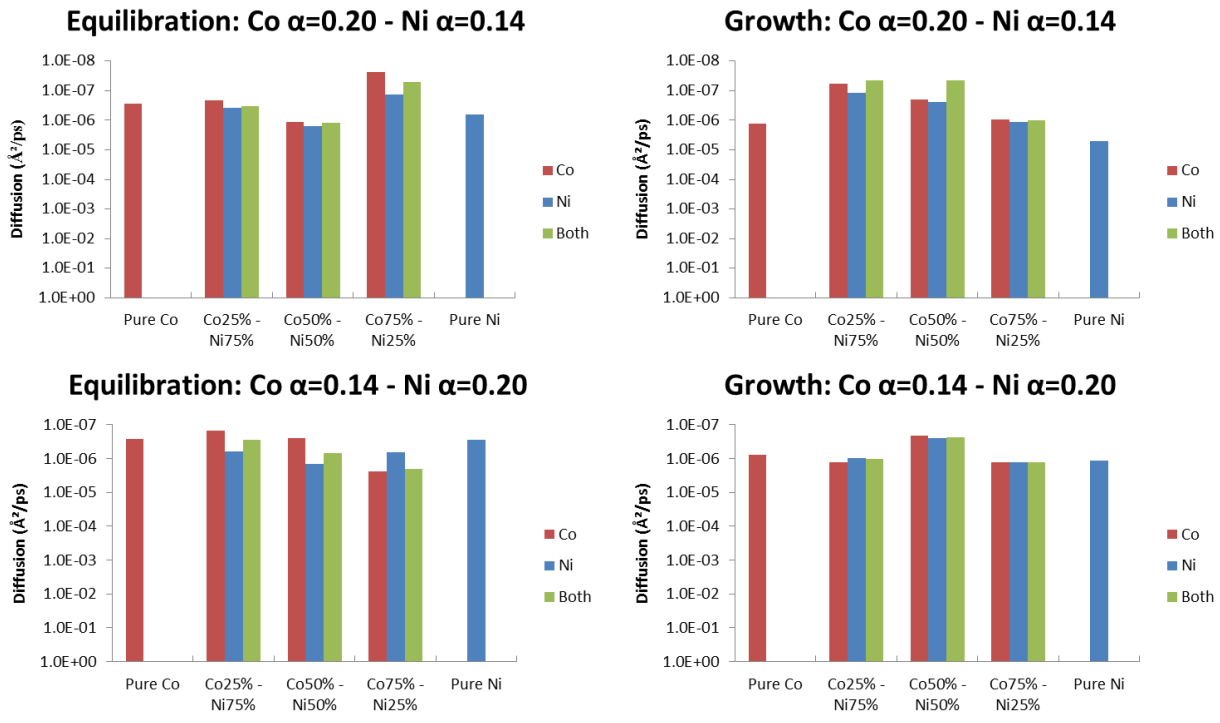

Figure 14. Diffusion coefficients (vertical axis) of metal nanoparticle atoms for equilibration and growth simulation phases for the set of alternating α-values 0.14 and 0.20.

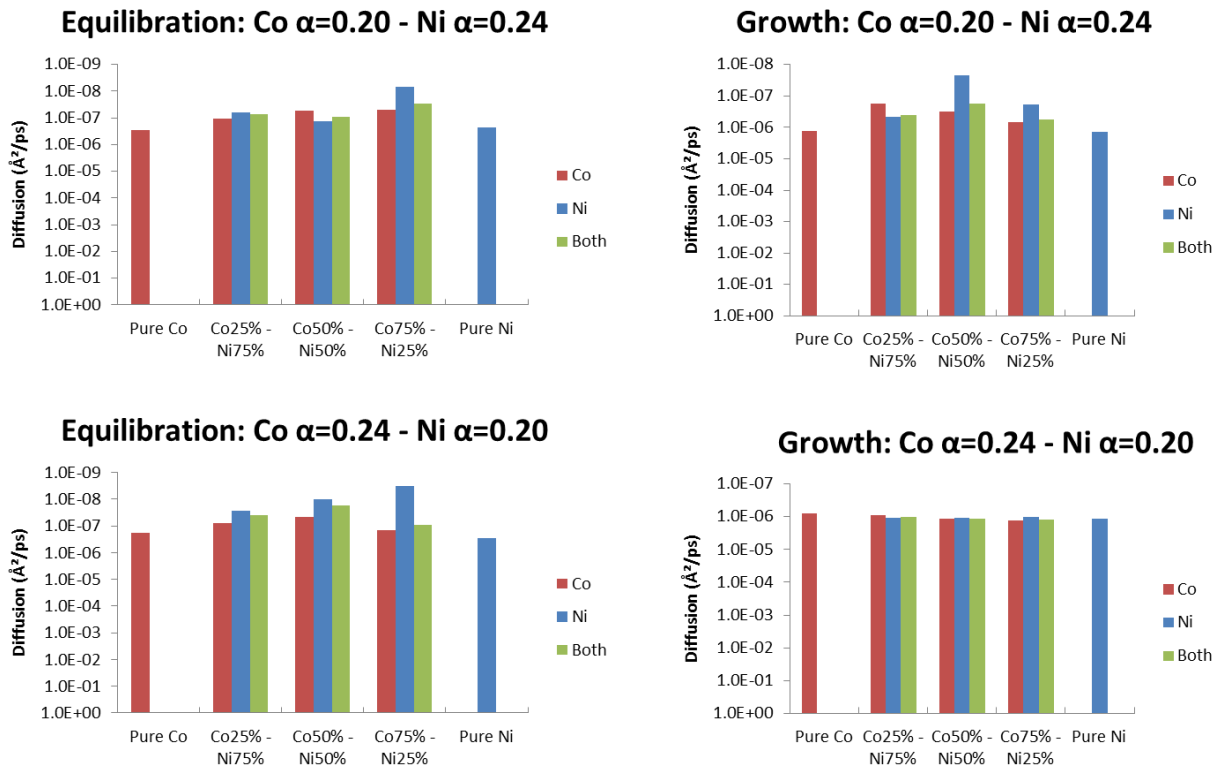

Figure 15. Diffusion coefficients (vertical axis) of metal nanoparticle atoms for equilibration and growth simulation phases for the set of alternating α-values 0.24 and 0.20.

Radial Pair Distribution Function graphs of the nanoparticle are represented for the growth simulation phase in Figure 16. As Co concentration increases, the Co-Ni coordination number is shown to increase. For example, at higher Ni concentration, there is more clumping of Ni-Ni and Co-Co. The other set of metal-support interaction simulations (not shown) suggested the same trend.

Density profile data with respect to the z-axis, the direction normal to the support, are presented in Figures 17 and 18. As seen through a comparison of pure nanoparticles, the effect of metal-support interaction is emphasized, with an increase in interaction resulting in higher density

closer to the support. The results suggest that nearly identical behavior is seen for Ni and Co at each combination of nanoparticle composition and metal-support interaction values.

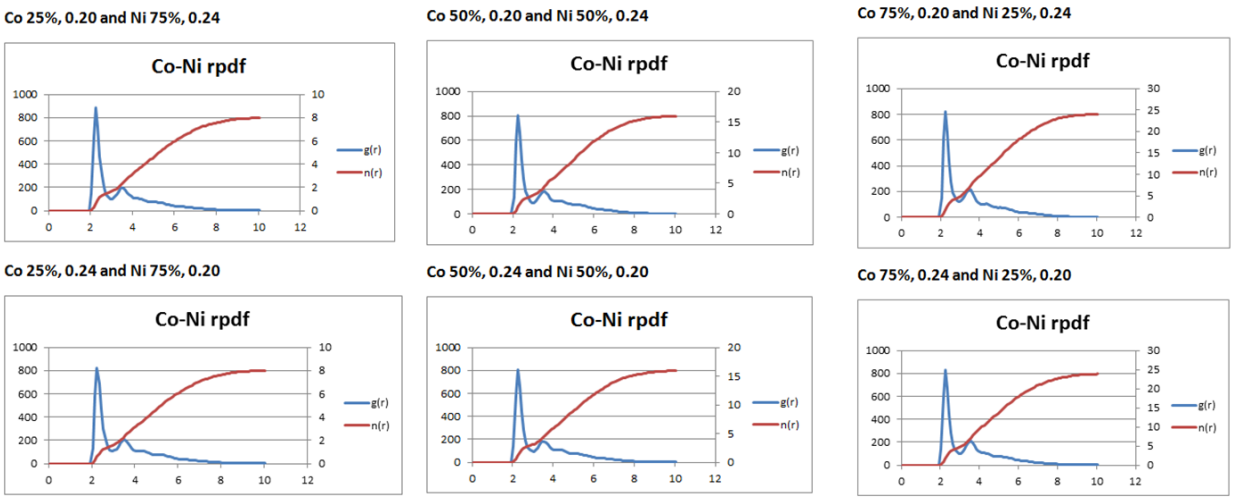

Figure 16. Radial Pair Distribution Function for the bimetallic simulation set of metal-support interaction values of 0.20 and 0.24.

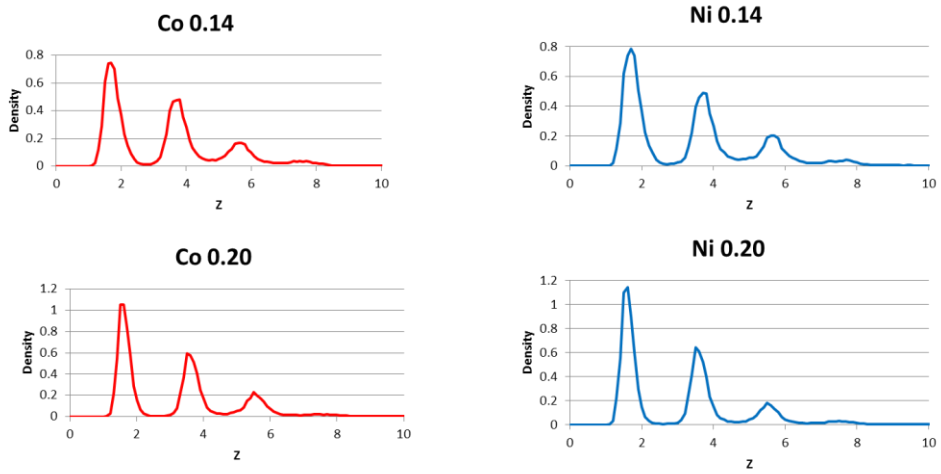

Figure 17. Z-density profiles calculated during growth for pure nanoparticles; Metal-support interaction values for each case are given above the graphs; Horizontal axis (z) is given in Å.

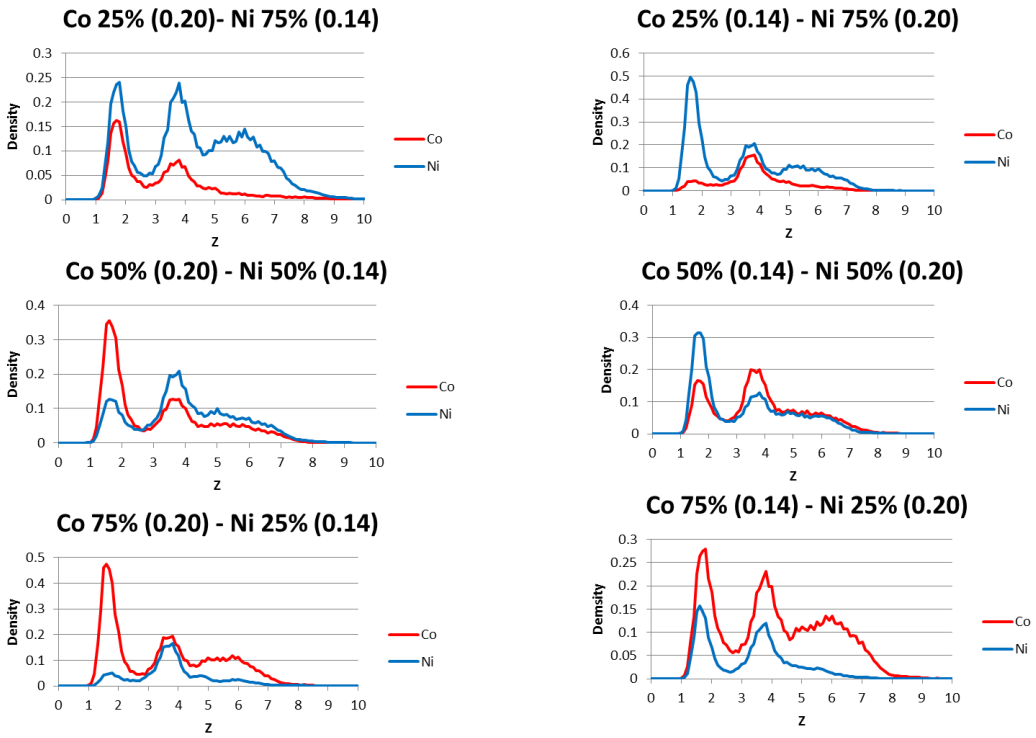

Figure 18. Z-density profiles calculated during growth for bimetallic nanoparticles. The z-axis is given in Å. Percent compositions and corresponding metal-support interaction values are displayed above each graph.

CHAPTER IV

CONCLUSIONS

To address the demand for a deeper understanding of SWCNT growth mechanism and the effects of key parameters thereof, this research project presents the analysis of various sets of simulation data. From the nature of the nano-catalyst state observed in the pure Ni cases, it is concluded that a carbide is not necessarily a prerequisite for carbon nanotube growth. This can be inferred from the formation of carbon chains within the nanoparticle, therefore negating the possibility of forming a carbide-like structure with C-Ni interactions. Furthermore, the previously observed flattening effect of high nanoparticle-support interaction on the nano-catalyst is confirmed.

Along with the faster catalysis rate of nanotubes grown using the C2 gas, a more prominent effect of nano-catalyst support interaction was observed for this precursor gas case. An increase in nano-catalyst support interaction strength was shown to facilitate faster incorporation of surface atoms into the nanotube cap network. These results indicate that the annealing effect may be less prominent when a dimer containing precursor gas is used, or at a higher nano-catalyst-support interaction energy.

In addition to lower nanotube quality resulting from the suppression of the annealing effect, stronger metal-support interaction was found to promote bamboo growth. This conclusion is valid throughout the pure and bimetallic nanoparticle cases. Furthermore, the bimetallic simulations indicated that both bamboo growth and horizontal growth were less likely to occur at

the low nano-catalyst-support interaction energies. This indicates that optimal growth conditions for high quality SWCNTs include a lower range of nano-catalyst/support interaction energies.

According to visual analysis of the bimetallic simulation set, the most frequently observed nucleating ring is a pentagon. This phenomenon agrees with the work of Morokuma et al. [10] and is desirable because of the pentagon-rich nature of the nanotube tip, as well as the likelihood of rearrangement to hexagons, as determined by this research group.

A final conclusion drawn from this research project is the observation of a higher surface carbon concentration at the interface areas of the Ni-Co bimetallic nano-catalysts. Further research must be conducted to determine whether this is a reoccurring phenomenon, and to investigate possible explanations and mechanisms for this occurrence.

REFERENCES

[1] I.F. Akyildiz, J. M. Jornet. "Electromagnetic Wireless Nanosensor Networks. ELSEVIER. Nano Communication Networks." *ELSEVIER. Nano Communication Networks* 1 (2010): 3-19. Print.

[2] Gómez-Gualdrón et al. "Dynamic Evolution of Supported Metal Nano-catalyst/Carbon Structure during Single-Walled Carbon Nanotube Growth." *ACS Nano* 6.1 (2012) Print.

[3] Juan C. Burgos, Erick Jones, and Perla B. Balbuena. "Effect of the Metal-Substrate Interaction Strength on the Growth of Single-Walled Carbon Nanotubes." *The Journal of Physical Chemistry* 115 (2011): 7668-7675. Print.

[4]] Martinez-Limia, A., J. Zhao, and P. B. Balbuena. "Molecular Dynamics Study of the Initial Stages of Catalyzed Single-Wall Carbon Nanotubes Growth: Force Field Development." *Journal of Molecular Modeling* 13 (2007): 595-600. Print

[5] D. A. Gómez-Gualdrón, J.M. Beetge, P.B. Balbuena. "Effects of Precursor Type on the CVD Growth of Single-Walled Carbon Nanotubes." *Submitted to J. Phys. Chem. C*, December 19, 2012. Print.

[6] Wu, J., et al. "Solid-State Synthesis of "Bamboo-Like" and Straight Carbon Nanotubes by Thermolysis of Hexa-Peri-hexabenzocoronene–cobalt Complexes." *Small* 1 (2005): 210-212. Print.

[7] Diego A. Gómez-Gualdrón, Jin Zhao, and Perla B. Balbuena. "Nano-Catalyst Structure as a Template to Define Chirality of Nascent Single-Walled Carbon Nanotubes." *The Journal of Chemical Physics* 134 (2011) Print.

[8] Hongwei Zhu, Kazutomo Suenaga, Jinquan Wei, Kunlin Wang, Dehai Wu. "A Strategy to Control the Chirality of Single-Walled Carbon Nanotubes." *Journal of Crystal Growth* 310.24 (2008): 5473-5476. Print.

[9] Odom, Teri Wang, et al. "Atomic Structure and Electronic Properties of Single-Walled Carbon Nanotubes." *Nature* 391.6662 (1998): 62. Web.

[10] Yasuhito Ohta, Yoshiko Okamoto, Alister J Page, Stephan Irle, Keiji Morokuma. "Quantum Chemical Molecular Dynamics Simulation of Single-Walled Carbon Nanotube Cap Nucleation on an Iron Particle." *ACS Nano* 3.11 (2009). Print.